Study of a Novel Isotropic Suspension Design for an Angular Gyroscope

Chris Painter* and Andrei Shkel**

Microsystems Laboratory, Department of Mechanical and Aerospace Engineering
University of California, Irvine, CA, USA
*cpainter@uci.edu, **ashkel@uci.edu, http://mems.eng.uci.edu

ABSTRACT

This paper describes the analysis of a novel isotropic suspension designed for use in a Micro Electro Mechanical System (MEMS) z-axis angular gyroscope. The suspension, consisting of six concentric interconnected rings rigidly attached to an anchored frame, supports a resonating proof mass whose line of oscillation precesses in the presence of rotation induced Coriolis force. The paper demonstrates that the studied suspension is robust to quadrature errors and minimizes structural energy losses. Using a strain energy method, a closed form solution for the effective stiffness is developed, which is confirmed using finite element modeling. A parametric analysis is used to verify the necessity of thick structural layers in the fabrication of the suspension in order to separate desirable and undesirable modes of vibration.

Keywords: MEMS Gyroscope, Angular Gyroscope, Isotropic Suspension, Structural Modeling of MEMS

1 INTRODUCTION

A MEMS angular gyroscope is a dynamic device that relies on resonance oscillation and the Foucault principle to measure angular displacements (Figure 1) [1]. While previous designs operated on the principle of vibrating shells [2], the studied device utilizes a vibrational "lumped mass system" with increased sense capacitance through the use of sense combs that are interwoven between the comb fingers of the proof mass.

The device operates by driving a proof mass into resonance along two orthogonal drive axes. Upon reaching the desired amplitude, the drive force is removed and the energy of the system is maintained using a specially designed control architecture [1], [3]. Rotation induced Coriolis force causes the line of oscillation to precess and the precession angle provides a direct measure of the device's angular displacement [4].

In the ideal operation of the gyroscope, the line of oscillation precesses (Figure 2a). This requires a suspension with equal stiffness along the principle axes of elasticity, or isotropic suspension. Operation of the gyroscope with a non-isotropic suspension results in quadrature error manifested as an elliptical oscillation pattern during precession (Figure 2b). This results in degraded performance of the gyroscope. In order to satisfy the isotropic condition, a novel concentric ring suspension consisting of six interconnected rings rigidly attached to an anchored frame [1] was studied.

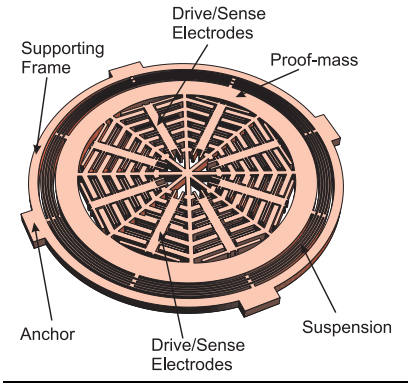

Figure 1: A MEMS angular gyroscope relies on resonance oscillation and the Foucault principle to measure angular displacements. A proposed suspension design consisting of six interconnected rings provides necessary isotropy required for the operation of this device.

The suspension is analyzed by utilizing strain energy methods to find a closed form expression for the stiffness of a single ring. The overall equivalent stiffness for the system is found through the superposition of each ring's stiffness in series. A finite element simulation of the suspension is then used to confirm the analytically obtained result. Finally, a parametric analysis of the suspension demonstrates the necessity for thick structural layers in order to prevent low frequency undesirable modes of operation.

2 ISOTROPY VERIFICATION

This section develops an analytical model to estimate the stiffness of the device's suspension system. The results are verified using finite element modeling.

2.1 Analytical Calculation

The system consists of a proof mass suspended above the substrate using six concentric rings (Figure 3a). The rings are interconnected at 90 degree increments and the outer ring is rigidly attached to an anchored frame. By calculating the deflection of the proof mass in response

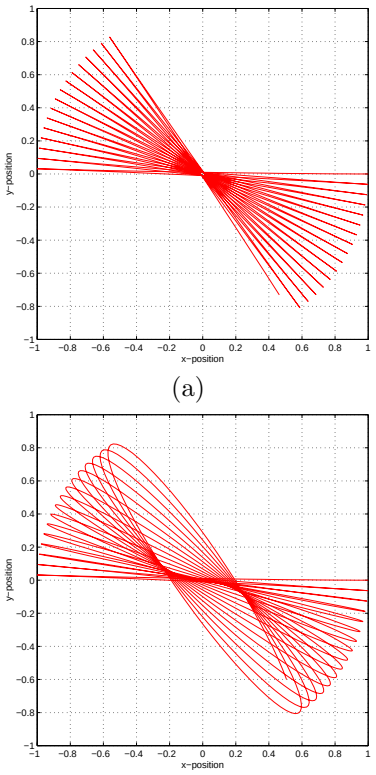

Figure 2: (a) An isotropic suspension allows the line of oscillation to precess. (b) A non-isotropic suspension results in quadrature error manifested as an elliptical oscillation pattern.

to a known arbitrary force $\vec{F}$ at an arbitrary angle α, an expression for the stiffness is found. The total deflection of the proof mass is then calculated by summing the contributions of each individual ring through superposition, assuming each ring interconnect is rigid.

We first find the deflection contribution of the inner ring. The inner ring is fixed at its connection points to the second ring and the rigid connection of the proof mass is modeled using constraint forces $(\lambda_1, \lambda_2, \lambda_3, \lambda_4)$ (Figure 3b). Due to symmetry, this model can be further decomposed to a quadrant of the ring (Figure 4) where the fixed end conditions at ends A and B are modeled using reaction forces and moments (R_x,R_y,M). M_0 represents the moment constraint assuming that the proof mass undergoes no angular deflection.

The corresponding reactions are calculated [5] as functions of the constraints and applied force and are used to find the total strain energy U of the curved member. If the radius r_1 is large compared to the thickness of the ring t, i.e. $\frac{r_1}{t} > 10$, the bending energy dominates the strain energy [5], and U can be expressed as

$$U = \int_0^{\frac{\pi}{4}} \frac{\hat{M}_A^2}{2EI}\, r_1 d\gamma \; + \int_0^{\frac{\pi}{4}} \frac{\hat{M}_B^2}{2EI}\, r_1 d\theta \tag{1}$$

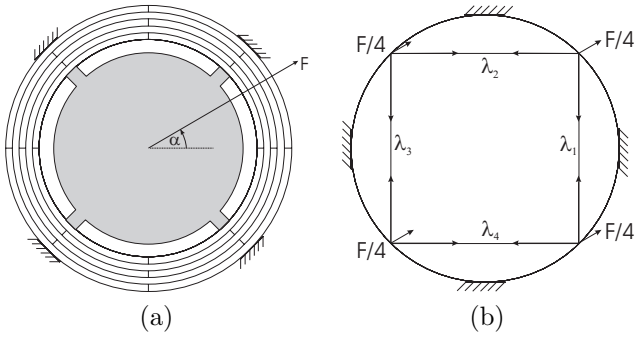

Figure 3: (a) The gyroscope is modeled as a proof mass suspended on a six interconnected ring suspension system. (b) The deflection of the proof mass due to a force $\vec{F}$ can be decomposed into the contributions of the inner ring and reactions from the subsequent rings.

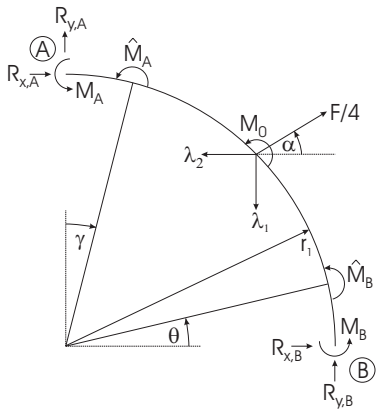

Figure 4: The deflection of the inner ring can be decomposed into the contributions of each quadrant. The λ's and M_0 represent constraint forces and a constraint moment due to the rigid attachment of the proof mass.

where

$$\hat{M}_A = -r_1(1-\cos\gamma)R_{x,A} - r_1 \sin\gamma R_{y,A} + M_A$$
$$\hat{M}_B = r_1 \sin\theta R_{x,B} + r_1(1-\cos\theta)R_{y,B} + M_B$$

$\hat{M}_A$ and $\hat{M}_B$ are the reaction induced moments at angles γ and θ from fixed ends A and B, respectively (see Figure 4). By Castiliano's theorem, the deflection of an elastic member in the direction of the applied force is equal to the change in strain energy with respect to the applied force [5],

$$\delta_{F,r_1} = \frac{\partial U}{\partial F} = \frac{r_1}{EI}\int_0^{\frac{\pi}{4}} \hat{M}_A \frac{\partial \hat{M}_A}{\partial F}\, d\gamma \; + \frac{r_1}{EI}\int_0^{\frac{\pi}{4}} \hat{M}_B \frac{\partial \hat{M}_B}{\partial F}\, d\theta \tag{2}$$

A similar solution is arrived at for each of the four quadrants, leading to a total of eight unknowns consisting of the four λ constraints and the four M_0 constraints. By

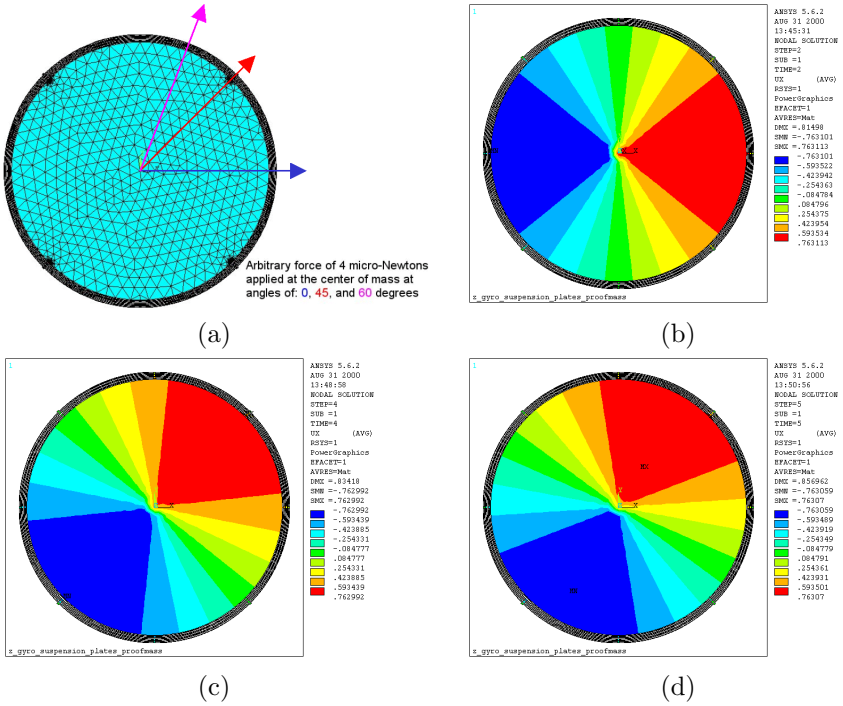

Figure 5: The uniformity of the suspension is confirmed by modeling the system using the FEM package ANSYS. The system is modeled using 3D shell elements. The proof mass is subject to the same load in the directions of (a) 0 ,45, and 60 degrees. The corresponding radial displacements as shown in (b), (c), and (d), respectively, are equal, which confirms the isotropy of the suspension.

assuming zero deformation in the constraints, the unknowns are eliminated by

$$\delta_{\lambda_1,UR} + \delta_{\lambda_1,LR} = \delta_{\lambda_2,UR} + \delta_{\lambda_2,UL} = 0$$
$$\delta_{\lambda_3,UL} + \delta_{\lambda_3,LL} = \delta_{\lambda_4,LL} + \delta_{\lambda_4,LR} = 0$$
$$\delta_{M_0,UR} = \delta_{M_0,LR} = \delta_{M_0,LL} = \delta_{M_0,UL} = 0$$

Here UR, LR, LL and UL designate the upper right, lower right, lower left, and upper left quadrants of the inner ring, respectively. Solving the system of equations simultaneously yields

$$\delta_{F,r_1} = \frac{r_1^3}{4EI}(4.017e^{-4}F) \tag{3}$$

We now find the contribution of the second ring by modeling it as rigidly attached where it would be connected to the third ring. The reaction forces of the inner ring are used as the applied forces on the second ring. Using the same solution procedure as for the inner ring, with the simplification that the second ring is unconstrained ($\lambda = M_0 = 0$), the deflection of the top and bottom quadrants of the second ring become

$$\delta_{F,r_2} = \frac{F}{EI}(.0002r_2^3\cos^2\alpha - .0001r_2^2r_1\cos^2\alpha + .0001r_2^3\sin^2\alpha) \tag{4}$$

We invoke a change of variable such that $r_1 = r_2 - \Delta r$, where Δr is the spacing between the rings. If the spacing is sufficiently small compared to the radius ($\Delta r \approx 0$), then (4) simplifies to

$$\delta_{F,r_2} = \frac{r_2^3}{4EI}(4.0104e^{-4}F) \tag{5}$$

With this simplification, the same result is found for the left and right quadrants. Assuming that the bending moment of inertia (I) and the modulus of elasticity (E) are identical for all rings, we see that this deflection varies only with radius when compared to the deflection of the inner ring (3). By induction, this expression for the ring deflection will propagate to each subsequent ring. The generalized stiffness can be approximated by force divided by deflection

$$k_r(r) = 9957.68\frac{EI}{r^3} \tag{6}$$

The total stiffness of the system can be approximated by summing the stiffness of all the rings in series

$$\frac{1}{k_{tot}} = \sum_{i=1}^{n}\frac{1}{k_i} \tag{7}$$

The final solution is not a function of α, so it is concluded that this stiffness is the same regardless of the angle of the applied force, thus verifying the isotropy of the suspension.

2.2 Finite Element Modeling

To verify the analytical calculation, a finite element model was constructed using the ANSYS multiphysics software package. The suspension and proof mass were modeled using three dimensional shell elements with a thickness of two microns (assuming surface micromachining technology). The radius of the rings used for simulation were 303.5, 306.5, 309.5, 312.5, 315.5, and 318.5μm and the width of each ring was 2μm. A known force of 4μN was applied at the center of the proof mass in three varying in-plane directions (0,45, and 60 degrees). The in-plane radial deflections of the proof mass were found to be the same in all three cases (Figure 5). Due to the symmetry of the structure, this demonstrates that the suspension is uniformly stiff in all radial directions. The stiffness, calculated as force divided by deflection, results in a value of 5.24 $\frac{\mu N}{\mu m}$. The analytical calculation gives a stiffness of 6.21$\frac{\mu N}{\mu m}$, yielding a difference of 15.6%. This discrepancy can be attributed to the use of shell elements in the finite element analysis.

3 MODE MATCHING

For the operation of the gyroscope, it is desirable to design the device where the operational modes are separated from the undesirable modes. Surface micromachining has limitations on the thickness of structural layers and these restrictions yield a low out-of-plane stiffness, resulting in undesirable low frequency out-of-plane modes (Figure 6). It is possible to compensate for this effect by utilizing thicker structural layers.

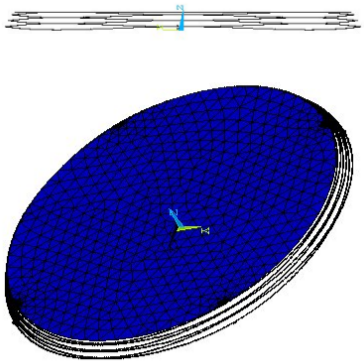

Figure 6: The use of thin structural layers in the design of the suspension results in low frequency out-of-plane modes.

As the thickness of the structural layer is increased, the in-plane bending moment of inertia, and therefore the in-plane stiffness of the rings, increases linearly ($k_r = f(t)$). In comparison, the out-of-plane moment of inertia, and thus the out-of-plane stiffness, increases as thickness cubed ($k_z = f(t^3)$). If the mass also increases linearly with thickness, the in-plane natural frequencies will remain constant ($\omega_n = \sqrt{\frac{k}{m}} = const$), while the out-of-plane natural frequencies will increase linearly ($\omega_n = \sqrt{\frac{k}{m}} = f(t)$).

From a parametric analysis of the suspension, at an optimal thickness of 20 microns, the out-of-plane stiffness is almost three times greater then the in-plane stiffness, thus providing an appropriate mode separation between desirable and undesirable modes of operation of the gyroscope.

4 CONCLUSION

In this paper, we have demonstrated that the proposed six concentric and interconnected ring suspension provides the necessary isotropy required for the operation of a MEMS angular gyroscope. We have developed a close form solution for the stiffness of the suspension, which is applicable towards any suspension of this type, given an arbitrary number of rings. It has also been shown that using a fabrication technology utilizing thick structural layers shifts the undesirable modes of operation to a higher frequency range, thus increasing the immunity of the device to undesirable excitations.

REFERENCES

[1] A. Shkel and R. T. Howe. Polysilicon surface micromachined rate integrating gyroscopes. UC-Berkeley Office of Technology and Licensing. Case Number B99-077.

[2] M. Putty and K. Najafi. A micromachined vibrating ring gyroscope. In *IEEE Solid State Sensors and Actuators Workshop*, pages 213–220, Hilton Head Island, SC, June 1996.

[3] A. Shkel, R.T. Howe, and R.Horowitz. Modeling and simulation of micromachined gyroscopes in the presence of imperfections. *International Workshop on Micro Robots, Micro Machines and Systems*, September/October 1999.

[4] A. Shkel, R. Horowitz, A. Seshia, and R.T. Howe. Dynamics and control of micromachined gyroscopes. In *The American Control Conference*, San Diego, CA, June 1999.

[5] Warren C. Young. *Roark's Formulas for Stress and Strain*. McGraw-Hill, Inc., 6th edition, 1989.